

Oxidative Precipitation as a Versatile Method to Obtain Ferromagnetic Fe_3O_4 Nano- and Mesocrystals Adjustable in Morphology and Magnetic Properties

Tim Granath, Peer Löbmann, and Karl Mandel*

Oxidative precipitation is a facile synthesis method to obtain ferromagnetic iron oxide nanoparticles from ferrous salts—with unexplored potential. The concentration of base and oxidant alone strongly affects the particle's structure and thus their magnetic properties despite the same material, magnetite (Fe_3O_4), is obtained when precipitated with potassium hydroxide (KOH) from ferrous sulfate (FeSO_4) and treated with potassium nitrate (KNO_3) at appropriate temperature. Depending on the potassium hydroxide and potassium nitrate concentrations, it is possible to obtain a series of different types of either single crystals or mesocrystals. The time-dependent mesocrystal evolution can be revealed via electron microscopy and provides insights into the process of oriented attachment, yielding faceted particles, showing a facet-dependent reactivity. It is found that it is the nitrate and hydroxide concentration that influences the ligand exchange process and thus the crystallization pathways. The presence of sulfate ions contributes to the mesocrystal evolution as well, as sulfate apparently hinders further crystal fusion, as revealed via infrared spectroscopy. Finally, it is found that nitrite, as one possible and ecologically highly relevant reduction product occurring in nature in context with iron, only evolves if the reaction is quantitative.

particularly important in water bodies and on iron-bearing surfaces, where oxygen or nitrate may act as oxidants. Especially the latter is in focus since the intensified agricultural use results in an increased release into natural waters. Reduction of nitrate can result in various products, depending on the reaction conditions.^[1,2,3–6] Thus, for example, the reduction products nitrite and ammonia, which are easily soluble in water, would be of great toxicological concern, especially for aquatic organisms.^[1,7] Similarly, nitrous gases that may arise can have likewise negative effects within the atmosphere.^[1,4,5,8,9]

The iron oxidation usually proceeds via a preliminary hydroxide stage (green rust), from which, in the end, more stable iron (hydr)oxides, such as goethite, lepidocrocite, ferroxhyte, ferrihydrite, or hematite, emerge in an initially nanoparticulate form.^[3,6,10–16] However, which product actually results, depends to a large extent on concentrations of the reactants,

pH value, temperature, type of oxidant, and ions/molecules present.^[6,11,13–18]


Due to the many possible influences, the seemingly simple reaction becomes very complex in detail. Consequently, the number of scientific disciplines that deal with this topic—and often focusing on completely different aspects—is correspondingly high. Thus, not only the resulting iron (hydr)oxides but also the associated processes and last but not least the generated reduction products play an important role. For example, in the fields of crystallography and mineralogy, the focus is on the formation processes and the crystalline properties of the resulting nanoparticulate products, especially with regard to appearance, purity, and periodicity.^[17,19] With regard to introduced, depleted, and released reaction components, environmental chemists, on the other hand, investigate the effects of such concentration changes on affected areas.^[4,20,21] At this point, also coordination chemistry comes into play since potential ligands present have a decisive effect on the reaction processes and thus also on the resulting products.^[22] In a more comprehensive view, the redox reaction is also directly related to the iron and nitrogen cycles, which are the focus of attention of (bio)geochemists.^[1,5,8,9,20,23] Much more application-oriented are the material scientists, who are not only interested in product properties but who also always have to consider possible aging processes and thus resulting durabilities.^[24] Similar interests are also pursued in

1. Introduction

The oxidation of iron—and especially iron(II)—is a process that takes place under natural conditions and, in this respect, is

T. Granath, Prof. K. Mandel
Department of Chemistry and Pharmacy
Inorganic Chemistry
Friedrich-Alexander University Erlangen-Nürnberg (FAU)
Egerlandstrasse 1, D91058 Erlangen, Germany
E-mail: karl.mandel@fau.de

T. Granath
Chair of Chemical Technology of Materials Synthesis
Julius-Maximilians-University Würzburg
Röntgenring 11, D97070 Würzburg, Germany
Prof. P. Löbmann, Prof. K. Mandel
Fraunhofer Institute for Silicate Research
ISC
Neunerplatz 2, D97082 Würzburg, Germany

 The ORCID identification number(s) for the author(s) of this article can be found under <https://doi.org/10.1002/ppsc.202000307>.

© 2021 The Authors. Particle & Particle Systems Characterization published by Wiley-VCH GmbH. This is an open access article under the terms of the Creative Commons Attribution License, which permits use, distribution and reproduction in any medium, provided the original work is properly cited.

DOI: 10.1002/ppsc.202000307

the field of colloidal and nanoparticle sciences, in which properties are studied that predominantly originate from very small particles and provide access to new materials and fields of application.^[25]

In order to simulate the processes in the laboratory and at the same time satisfy the requirements of all fields, a method reducible to a few parameters and requiring as little effort as possible would be ideal. A method that fulfills these demands is the oxidative precipitation of iron (hydr)oxides, which, of course, has been known for almost 100 years,^[26] but received increased attention only since the very detailed description by Sugimoto and Matijeć.^[3] Typically, the method involves two steps. While the first step concerns the generation of a preliminary hydroxide stage, the second step aims to convert the preliminary stage into more stable iron (hydr)oxides through an aging process.^[3,27] The simplicity of the method enables intensive investigations under easily parameterizable conditions, which can even go beyond the limits of nature. For example, the generation of magnetite can be increased by increasing the temperature. Since magnetite is a material of special interest, mainly because of its magnetic properties in combination with its toxicological harmlessness, the focus of material science studies is often on the synthesis of this iron oxide. In this respect, a number of investigations can be found which, for example, deal intensively with the influence of the pH value, the type of oxidant, the temperature, or the ions present.^[3,6,11,12,15–17,28,29,30,31] Unfortunately, information about the role of nitrate concentration can rarely be found.

With regard to the formation of magnetite, the present study, therefore, deals in detail with the relationship between nitrate and hydroxide concentrations. In this respect, the main interest is the influence on morphological appearances and magnetic properties. Furthermore, the arising reduction products, as well as a possibly more important role of the anions present, are also taken into account in the interpretation of the results.

2. Theoretical Model

In this study, the investigated parameters are the hydroxide and nitrate concentration, which are related to the amount of ferrous iron that is used. Both species concentrations and relations to iron(II) are expected to matter in certain concentration fields, as outlined in the following theoretical considerations.

2.1. Theoretical Considerations Regarding the Hydroxide to Iron(II) Ratio

In order to take the hydroxide concentration into account, factors that refer to its excess over Fe^{2+} or that simply put the species (Fe^{2+} , OH^-) in relation to each other can be employed (see Section 1 in the Supporting Information).^[3,12,14–16,29,32] For our purposes, it is advantageous to combine both approaches, and, in addition, taking into account any proton concentration present. Accordingly, the ratio R_{OH} used herein to consider the hydroxide concentration is given by the following Equation (1):

$$R_{\text{OH}} = \frac{[\text{OH}^-] - [\text{H}^+] - 2 \cdot [\text{Fe}^{2+}]}{[\text{Fe}^{2+}]} \quad (1)$$

Assuming that there may be a relationship between coordination and conversion of Fe^{2+} , two values of R_{OH} are of particular importance. The first one is $R_{\text{OH}} = 0.0$. At this point, the charges resulting from the concentrations of OH^- , Fe^{2+} , and H^+ are balanced. As described in literature, oxidation takes place via various hydroxide intermediates originating from $\text{Fe}(\text{OH})_2$.^[3,10–12] At $R_{\text{OH}} \geq 0.0$, this should stoichiometrically be fulfilled quantitatively for all used iron(II) as long as no stronger ligand is available that would otherwise complex the iron(II) (which is not the case in the synthesis considered herein).

For values of $R_{\text{OH}} < 0.0$, no quantitative conversion of iron(II) via oxidation of formed $\text{Fe}(\text{OH})_2$ to iron oxide can be expected. Consequently, for $R_{\text{OH}} < -2.0$ no precipitation at all will occur. Thus, $R_{\text{OH}} = -2.0$ marks the second important value to be considered.

2.2. Theoretical Considerations Regarding the Nitrate to Iron(II) Ratio

Although there are sporadic notes in the literature, there is, as far as we know, no empirical study, investigating the relationship between nitrate and iron concentration with respect to product evolution of magnetic iron oxide due to oxidative precipitation. Since no trivial dependencies are known, we introduce a parameter R_{Ox} and keep it simple (Equation (2)):

$$R_{\text{Ox}} = \frac{[\text{NO}_3^-]}{[\text{Fe}^{2+}]} \quad (2)$$

It is important to note that this, at first glance quite a simple relationship, unfortunately, disguises the fact that the reduction path of nitrate can vary greatly (Scheme 1 and Section 2 in the Supporting Information).

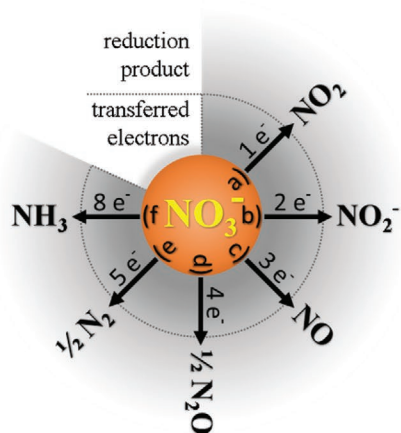
As shown, depending on the reduction pathway, different minimum amounts of nitrate—expressed as $R_{\text{Ox,min}}$ —are required to stoichiometrically oxidize iron(II) to Fe_3O_4 .

Accordingly, several problems have to be considered: Not only does the reaction pathway determine the nitrate consumption alone, but also the associated proton release and, last but not least, the resulting reduction product. Predicting the actual reaction pathway is almost impossible.

In order to handle this complexity, we focused on the pathways where nitrite, or ammonia, arise, respectively, since these can be determined rather easily. Assuming this, in order to obtain Fe_3O_4 stoichiometrically from iron(II), the values of $R_{\text{Ox,min}} = 0.33$ (Scheme 1 reduction path (b)) and $R_{\text{Ox,min}} = 0.08$ (Scheme 1 reduction path (f)) result, respectively. Interestingly, the corresponding nitrate concentrations are therefore much lower than those, usually reported in literature.^[3,12,28,29,31,32] In order to point out a possible correlation, values with a certain relationship to reduction paths therefore serve as starting points for the experiments and receive special attention concerning the interpretation of the results.

3. Results and Discussion

To approach the complex processes during particle evolution in the precipitation–oxidation synthesis in order to understand



Nitrate reduction path	eq. NO ₃ ⁻ consumption ¹	eq. H ⁺ release ²	R _{Ox,min}
a) NO ₂	120	240	0.67
b) NO ₂ ⁻	60	360	0.33
c) NO	40	320	0.22
d) N ₂ O	30	330	0.17
e) N ₂	24	336	0.13
f) NH ₃	15	345 ³	0.08
O ₂ as oxidant	30 eq. O ₂	360	-

¹ to obtain 60 equivalents Fe₃O₄ from 180 eq. Fe²⁺

² reaction in H₂O, assuming Fe²⁺ as the reactive species

³ 330, if NH₄⁺ as reduction product is the basis of calculation

Scheme 1. Typical reduction pathways of nitrate, together with the stoichiometric amount of nitrate required, the resulting proton release, and the corresponding R_{Ox}-value to obtain 60 equivalents of Fe₃O₄.

how the synthesis conditions influence the resulting particle morphologies that ultimately control their magnetic properties, the organization of experiments and description of their results is as follows:

At first, based on preliminary experiments, syntheses observations, depending on R_{OH} and R_{Ox} in general are revealed and time-dependency of the product evolution is studied (Section 3.1). Next, a detailed electron microscopy study of obtainable particle morphologies, based on distinct R_{OH} and R_{Ox} regions, is described (Section 3.2), followed by a discussion of the particles' composition and chemistry (Section 3.3). The findings from these chapters not only made it possible to explain the evolution of either nano- or mesocrystals but also to define specific reaction condition regions that clearly correlate with certain particle morphologies (Section 3.4). Eventually, the different conditions could be related to the particles' magnetic properties, which are determined by the particle morphologies (Section 3.5).

3.1. Synthesis Observations and Product Evolution with Time

Since, according to literature, magnetite can only be obtained as an oxidation product from a ferrous species above a certain temperature, all syntheses were performed at elevated temperature and this parameter was not investigated further.^[3,15,33] The ideal basic synthesis procedure was identified as to dissolve ferrous sulfate in deionized water and heat it up to boiling under reflux in a nitrogen atmosphere before adding the alkaline oxidation solution, that is, an aqueous solution containing both, the base KOH and the oxidant KNO₃ in a premixed aqueous solution.

Despite the reaction is simple and involves only three chemicals, the addition order, and timing matters, as it was found in preliminary experiments (see Section 3 in the Supporting Information). This indicates that it is crucial to understand the details in order to be influenced to control the reaction.

To study the influence of hydroxide and nitrate in detail, that is, to understand how R_{OH} and R_{Ox} influence the reaction product, respectively how R_{OH} and R_{Ox} can be used to group or classify the synthesis result, KOH and KNO₃ were systematically varied in concentration, while the iron

concentration was fixed at 20 mM. At the end of each reaction, the precipitate was separated and the pH value was measured in the supernatant. Furthermore, also the amount of dissolved iron and dissolved nitrite was determined quantitatively, respectively semi-quantitatively.

3.1.1. The Role of R_{OH}

While no dissolved iron was found at R_{OH} ≥ 0.0, the amount of iron found for R_{OH} < 0.0 increased steadily with decreasing R_{OH}. The determined values are plotted in Figure S1a, Supporting Information. The findings fit quite well with the hypothetical assumption that the precipitation of iron (hydr)oxides is strongly associated to the presence of an equivalent amount of hydroxide in the order of [OH⁻]:[Fe²⁺] = 2:1. Furthermore, this relationship appears to be independent of the nitrate concentration, since a change in this regard did not result in significantly different levels of residual iron in solution.

This nitrate-independency seems to apply equally to the pH value evolution, as the measured values of corresponding experiments are nearly identical, respectively indistinguishable, within the measurement error (Figure S1b, Supporting Information). Therefore, it can be assumed that the reaction does not exclusively follow one path, since then, more significant differences would be expected due to the unequal proton release. Rather, it seems more likely that the reaction proceeds through different stages, which in turn may be accompanied by different reduction processes.

The validity regarding the predicted transition points at R_{OH} = -2.0 and R_{OH} = 0.0 is very well supported by the results of the iron residue determination. However, this is not easy to comprehend on the basis of the data from the pH measurements, as they indicate a value around R_{OH} = -0.2 with respect to the quantity point, which is slightly below the predicted value of R_{OH} = 0.0. An explanation for the shift could be that the pH value decreases due to a possible hydrolysis of the remaining dissolved iron.

However, from our point of view, it is reasonable to state that in principle two clear transition points exist: this is on one hand

the point $R_{OH} = -2.0$: Below this point no reaction takes place. On the other hand, it is the point $R_{OH} = 0.0$: While above this point the precipitation is quantitative, it terminates by itself due to an equivalent consumption of OH^- for values of $R_{OH} < 0$, which is clearly indicated throughout a drop of the pH value.

3.1.2. The Role of R_{Ox}

In order to make a statement regarding possible correlations concerning the nitrate concentration, the following must be considered: The R_{Ox} dependency in the “non-quantitative region”, that is, where $R_{OH} < 0.0$, is difficult to assess. It is necessary to distinguish between the R_{Ox} that is based on the actually used $[Fe^{2+}]$ and the R_{Ox} associated to the maximum of convertible Fe^{2+} related to the initial $[OH^-]$. In the “non-quantitative region” the used $[NO_3^-]$ is in any case higher than the necessary concentration predicted due to the stoichiometry-calculation. Since there is no clarity about the reaction path finally taken, it is inappropriate to assume the values of the simple ratio R_{Ox} as a basis for deriving possible relations. This is especially valid for very small R_{OH} and/or large R_{Ox} values.

In the “quantitative region”, that is, where $R_{OH} \geq 0.0$, clear correlations can be made—it was found that the nitrate concentration has an effect on the resulting product. At the lowest tested value of $R_{Ox} = 0.15$, besides magnetite as the synthesis product and presumably ammonia or nitrogen as possible reduction products, a by-product is generated. Its presence can be related to the existence of a band at about 800 cm^{-1} in the corresponding infrared spectrum (Figure S2a, Supporting Information). The by-product, which appears as hexagonal platelets

in the scanning electron microscopy (SEM) (Figure S2b, Supporting Information), was identified as ferrosityte based on X-ray diffraction (XRD) analysis (Figure S3a1, Supporting Information). However, already slightly above this concentration, at $R_{Ox} = 0.25$, the band no longer appears in the infrared spectrum (Figure S2a, Supporting Information). Also, no by-product could be identified in the SEM images (Figure S2b, Supporting Information). At this nitrate concentration, it is stoichiometrically also conceivable that nitroxides are formed as reduction products. Surprisingly, besides the also detected gaseous ammonia, a small amount of nitrite was found in the supernatant. This can be taken as a clear hint that the formation of magnetite under these conditions is not necessarily related to only one reduction process.

3.1.3. Product Formation Evolution with Time in Dependence of R_{OH}

Having identified the conditions for the two most distinct synthesis parameter regions, namely the “non-quantitative region” at $R_{OH} < 0.0$ and the “quantitative region” at $R_{OH} \geq 0.0$, the factor time was studied for reactions in these two regimes and a time-dependent evolution of the product formation was discovered by studying the product with SEM (Figure 1).

For $R_{OH} \geq 0.0$ (in Figure 1 exemplarily shown for $R_{OH} = 1.1$), that is, in the “quantitative region”, once magnetite formed from the precipitation–oxidation reaction, no more time-dependent change was observed. The magnetite formation itself from the initial precipitation–oxidation reaction occurred in general comparably fast within the first two hours, depending on the

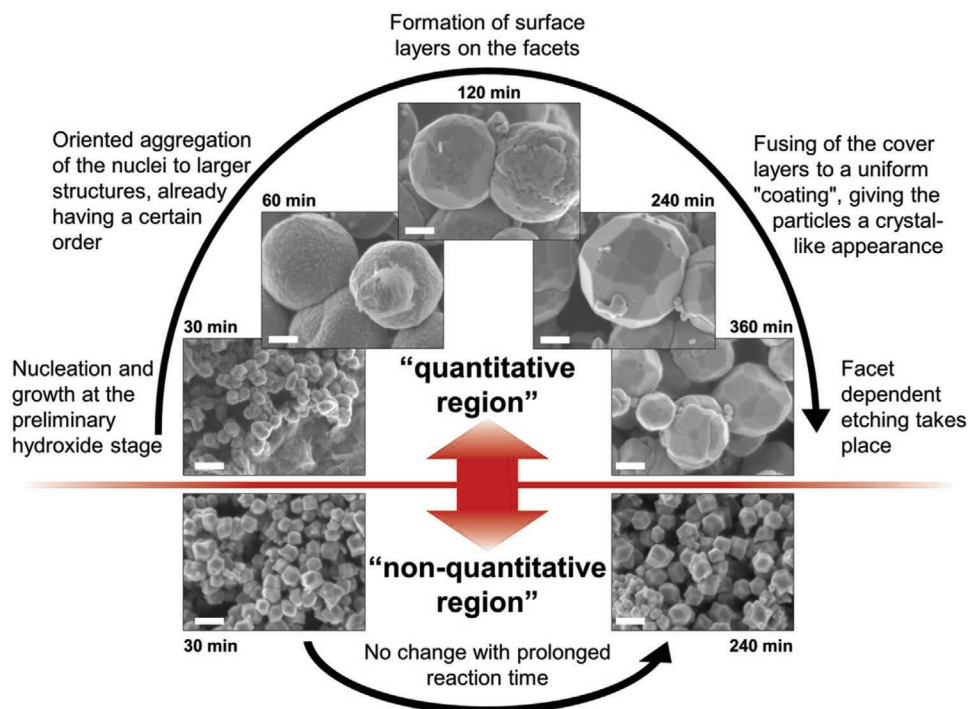


Figure 1. Time-dependent evolution of magnetite nanoparticles in the “quantitative” and “non-quantitative region” exemplary for the syntheses at $R_{OH} = 1.1$ and $R_{OH} = -0.7$, respectively. R_{Ox} is set to 1.4. Scale bars are 200 nm.

amount of nitrate used (the more nitrate provided, the faster the formation was).

For $R_{OH} < 0.0$ (in Figure 1 exemplarily shown for $R_{OH} = -0.7$), that is, in the “non-quantitative region”, however, the reaction time is crucial. Based on the impressions from the SEM images, it may be assumed that after nucleation, some kind of aggregation takes place, yielding large mesocrystal-like particles, however without clearly pronounced facets. As the reaction time proceeds, the surface of the particles gradually changes. The previously rough appearance undergoes some kind of smoothing and facets get more pronounced. As the process continues, the entire particle surface is finally straightened and all facets become clearly visible. After about 240 min, this transformation yields a polyhedral structure with relatively sharp and easily recognizable facets.

From the described observations and drawn conclusions up to this point, it cannot be stated which particular process actually causes this, but there seems to be a connection between the nitrate concentration and the resulting facet number, which will be discussed later. It is also unclear whether this process is only limited to the surface or also takes place within the cluster.

The finding that certain reaction conditions cause particle morphologies to evolve only if sufficient time is provided, was considered in all further experiments: In all cases, the time was set to 240 min in order to allow the systems to reach their presumable thermodynamically most favorable shape.

It is worth noting that if the reaction time was significantly further prolonged, the growth process partly reverts, as seemingly, etching takes place; yet affecting specific facets, only (see Section 4 in the Supporting Information for a more detailed discussion).

3.2. Appearance/Morphology

The following in-depth studies regarding achievable particle morphologies with varying R_{OH} and R_{Ox} conditions were made, based on the above-described findings, in thermodynamic equilibrium, that is, all reactions were given a time of 240 min to ensure that the most stable particle morphology could evolve.

Depending on the R_{OH} value, as described, basically two regions can be distinguished, namely the “non-quantitative region” and the “quantitative region” which are clearly separated by the quantity point at $R_{OH} = 0.0$. Both regions can in turn be divided into two further regions if the amount of nitrate used, expressed by the parameter R_{Ox} , differs significantly (Figure 2).

Thus, for $R_{OH} < 0.0$, the “non-quantitative region”, relatively large polyhedral particles are obtained. While the particles are pentacantahedral (50 facets) when a small amount of nitrate is used (Figure 2a2,e1), which corresponds to a low R_{Ox} , they become dodecahedral (12 facets; Figure 2(b2,f1) when R_{Ox} is high. If in both cases R_{OH} is quite low (< -1.0), the resulting particles appear more clustered (Figure 2a1,b1). However, they seem to retain their respective facet numbers.

For $R_{OH} \geq 0.0$, the “quantitative region”, there is no major similarity. Again, if the R_{Ox} value is low, the particles obtained are quite large (Figure 2c1,c2,e4). However, they are much less well-defined, which makes it more difficult to distinguish any facets that may exist. The recognizable ones range from

dodecahedral- to octahedral-like. If R_{OH} is increased in the low R_{Ox} -region, ferroxhyte, in the shape of hexagonal platelets, is precipitated as well (Figure 2c3). Furthermore, it becomes the dominant product at very high R_{OH} or when R_{Ox} is set even lower. In contrast, if R_{Ox} is high, presumably single octahedral crystals are obtained (Figure 2d1–d3), whereby the choice of R_{OH} seems to have little influence in this respect.

A more detailed analysis around the transition point $R_{OH} = 0.0$ reveals an additional “third” region where the particle morphology seems to be very sensitive towards changes in concentration and gives rise to new particle types. Thus, the particles obtained within the low R_{Ox} -region, are still large but now octadecahedral (18 facets; Figure 2e2,e3). Right at the transition point and slightly above, small dodecahedral crystals (Figure 2f3,f4) were obtained when the precipitation was carried out within the high R_{Ox} -region. Under the same conditions, but slightly below the transition point, also rod-like crystals were obtained (Figure 2f2), which were identified as goethite based on XRD analysis (Figure S3a2 in the Supporting Information). The amount of goethite obtained seems to correlate with the amount of nitrate used, in the sense that with increasing R_{Ox} also the quantity of goethite increases and vice versa.

3.3. Detailed Material Analysis Based on XRD and FTIR

Figure 3 shows a dedicated selection of powder diffractograms (XRD) and Fourier transformed infrared spectra (FTIR) of the particles obtained for the different regions (as discussed in Section 3.2).

According to the diffractograms, in almost all cases, magnetite is the only product identifiable. Throughout the entire R_{OH} – R_{Ox} range tested, only two additional precipitates were obtained. One was goethite, which was found only in a very small region slightly below the transition point ($R_{OH} = 0.0$), as long as R_{Ox} was sufficiently high. The other one was ferroxhyte, for R_{OH} being relatively high while R_{Ox} being rather low. Ferroxhyte is difficult to identify using XRD due to its amorphous character. However, if it is present in sufficient quantity, it can be well distinguished, particularly by two broad bands that appear around $2\theta = 40.5^\circ$ and $2\theta = 54.1^\circ$.

The calculation of the crystallite sizes using the Scherrer equation resulted in diameters in the size range of about 20 to 50 nm (Figure S4, Supporting Information). This fits quite well with the impressions from the SEM images (see Figure 2) of the presumably single-crystalline products obtained when R_{OH} is above the transition point and also R_{Ox} being relatively high. But, basically, it does not fit for all other particles, as they were found to be in the size range from 100 to 400 nm. This discrepancy supports the hypothesis that these larger particles are potentially mesocrystals.

Ferroxhyte, goethite, and magnetite can also be distinguished quite effectively using infrared spectroscopy (Figure S3c1–c3, Supporting Information). Thus, ferroxhyte, obtained in the high- R_{OH} -low- R_{Ox} -region, shows a broad OH band around 800 cm^{-1} and an Fe–O band around 425 cm^{-1} .^[34] Goethite, obtained as a by-product at $R_{OH} = -0.1$ and at $R_{Ox} \geq 3.5$, exhibits, besides an Fe–O band around 625 cm^{-1} , a very characteristic intense and sharp double band at 900 and 795 cm^{-1} .^[34] Pure magnetite, instead, should basically show only one Fe–O band at about

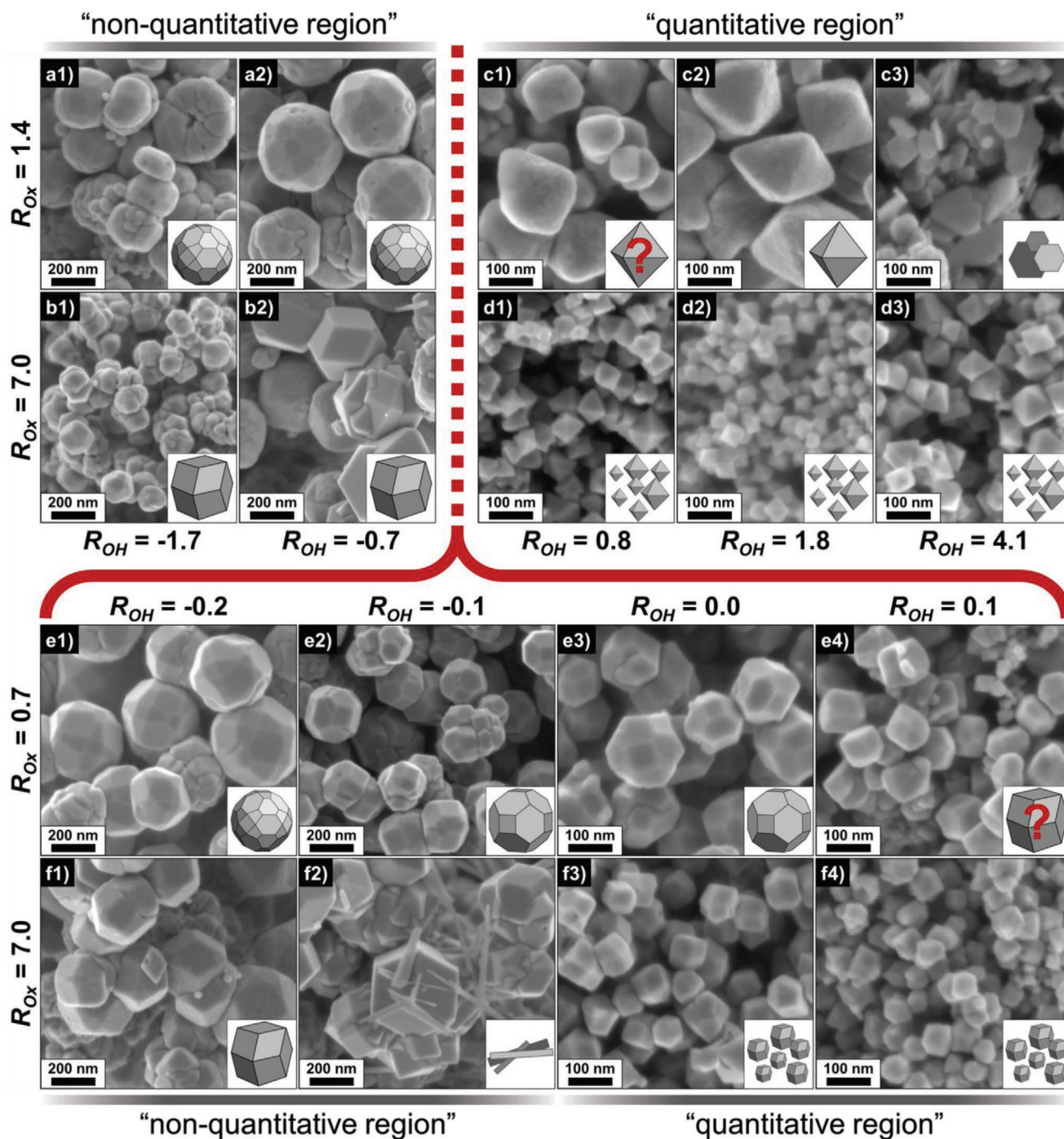


Figure 2. SEM images depicting the particle morphology obtained for different R_{OH} and R_{Ox} conditions.

570 cm^{-1} in the 4000–400 cm^{-1} region.^[35,36] Additional bands may appear, indicating residual water. Typically, these can be found around 1630 and 3400 cm^{-1} .^[35] Yet, in fact, only the spectra of the products obtained between $R_{OH} = 0.0$ and $R_{OH} = 1.0$ at high R_{Ox} correspond to this. In every other case, there are significant differences, which can be associated with two main causes:

The first occurs almost exclusively only with magnetite, which, regardless of the chosen R_{Ox} , was obtained within the "non-quantitative region" ($R_{OH} < 0.0$). In the infrared spectrum,

it appears as a triplet with maxima at about 1120, 1040, and 975 cm^{-1} . This triplet can be very well associated with the presence of a sulfate group and is, in this way, also typical for sulfate-containing iron oxides such as schwertmannite.^[37] This finding would fit well with the assumption that the products could be mesocrystals, since a sulfate group would be capable enough to act as a spacer between the crystallites, thus preventing their fusion. It may also explain why the obtained products appear more clustered when the R_{OH} decreases

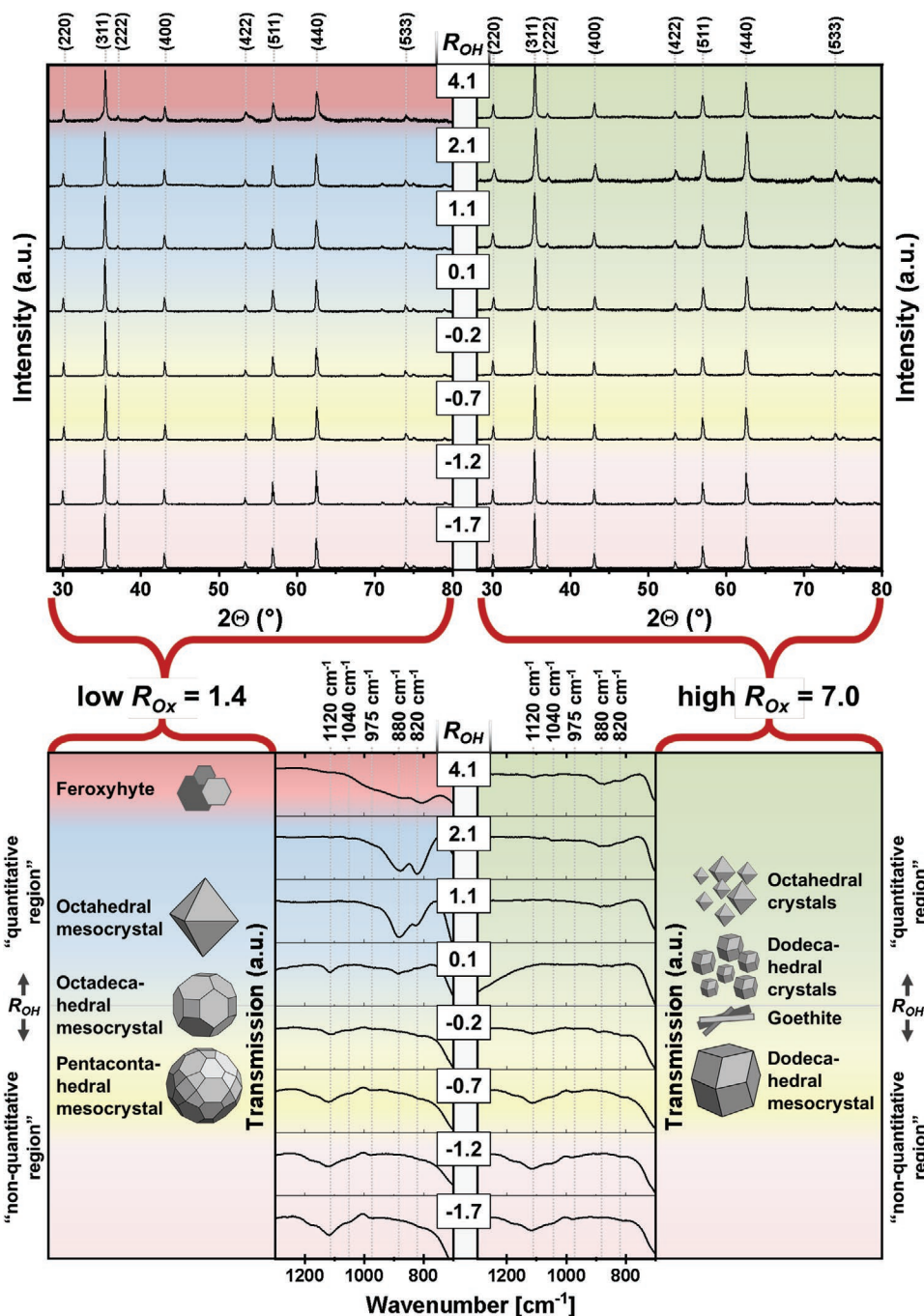


Figure 3. XRD (top) and FTIR (bottom) spectra of the obtained products as a function of R_{OH} at low (left-hand side) and high (right-hand side) R_{Ox} . In the XRD, the most intense magnetite bands are labeled. In the FTIR spectra, characteristic bands of attached molecules are labeled.

further. Thus, ligand exchange processes could be significantly slowed down and consequently, possible fusion processes more strongly impeded.

The second cause for a deviation in the FTIR spectra from the expected ones according to literature is indicated by a doublet at about 880 and 820 cm^{-1} and occurs mainly with magnetite obtained within the "quantitative region" ($R_{OH} \geq 0.0$) within which sulfate as a ligand should presumably no longer

be involved. This doublet can be associated with ion-coordinated OH and is, for instance in this way, often observed for clay minerals such as smectites.^[38] In contrast to the spectra associated with sulfate, the spectra of low and high R_{Ox} differ significantly. Thus, in the first case, the bands appear with a much higher intensity than in the second, where they are hardly visible. This difference can be correlated with the size and structure of the resulting particles. Since the products, which are

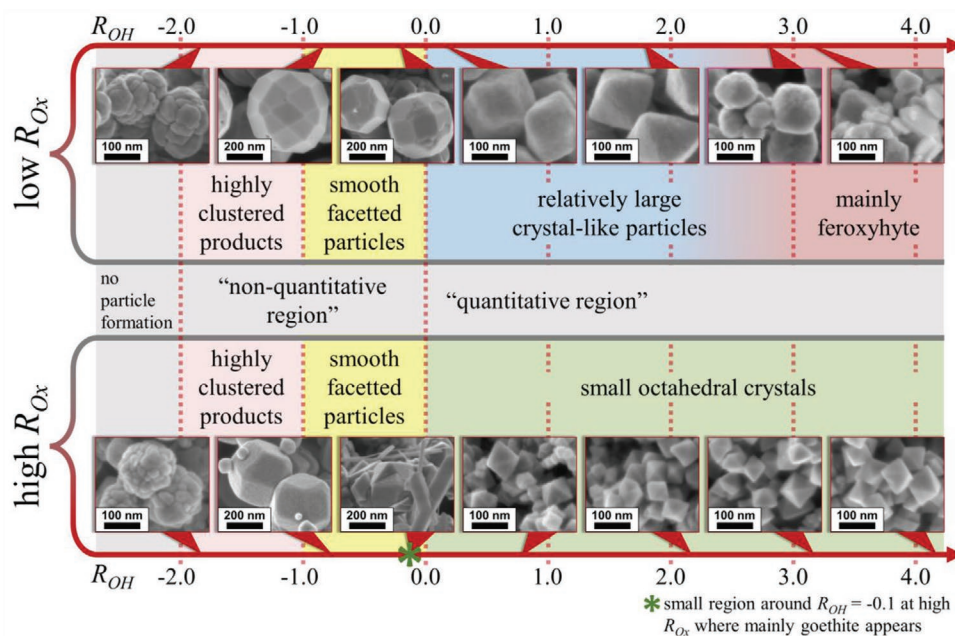


Figure 4. Assignment of the obtained particle morphologies to regions that can be delimited by integer R_{OH} -values.

obtained by using only a small amount of nitrate, appear as some kind of a mesocrystal, they have to be imagined as relatively large aggregates containing something that hinders further fusion. This obstacle, in this case, could now be the coordinated OH. At $R_{Ox} \geq 7.0$ instead, the obtained particles are very small (see Figure 2d1–d3,f3,f4) and, according to the XRD evaluation, almost single crystals. Consequently, OH is not trapped and thus also more easily exchangeable. With increasing R_{OH} , however, the OH exchange becomes more difficult, thus, causing the intensity of the corresponding bands to increase.

Since it can be assumed in principle that both, sulfate and hydroxide, have an influence on the surface charge, the zeta potential was measured as a function of the pH value to determine the isoelectric point (IEP). According to literature, the IEP of magnetite typically ranges from pH 6.4 to 8.^[39] In case of sulfate or hydroxy groups dominating the surface, a shift of the IEP towards lower pH values would be expected in both cases. However, no strong shift could be observed (Figure S5, Supporting Information). The values determined range from about pH 5.5 to 6.5, which is slightly below the values found in literature. Despite the fact that the shift is relatively small, it is basically in accordance with the expectations, so that it is reasonable to assume that the particles that are obtained do not possess a “perfectly pure iron oxide character” at their surface. However, with respect to the examined parameters, no distinct trend could be observed, since the values are too close together. Merely, the consistent drop at the transition point $R_{OH} = 0.0$ to the “quantitative region” is conspicuous. However, this drop fits well with the previous results, as from that point on, clearly different products result.

3.4. Multiples and Reduction Products

The results so far indicate that there seem to be some relatively sharp demarcation points that coincide remarkably well

with integer multiples of the R_{OH} -values and could therefore possibly be associated, for example, with ligand coordination (Figure 4).

The most obvious ones are, of course, both transition points at $R_{OH} = -2.0$ and $R_{OH} = 0.0$. While the former is the point at which precipitation is initiated in the first place, the latter marks the quantitative threshold. Between these two points, the reaction is not quantitative. It stops due to the self-consumption of the necessary hydroxide. That means the reaction terminates itself. Accordingly, this is generally accompanied by a significant drop in pH value, which, in the “non-quantitative region”, usually ends in the acidic pH region. Also, there is another, more subjective point in this region, which is around $R_{OH} = -1.0$. Below this point, the particles are much more strongly clustered, whereas above it they appear relatively homogeneous. Furthermore, regardless of the amount of nitrate used, basically, no nitrite could be determined in the “non-quantitative region” after the reaction had finished (Figure 5).

In this respect, the only exception was the range between $R_{OH} = -0.2$ and $R_{OH} = 0.0$. While the determined nitrite concentration at $R_{OH} = -0.2$ reached a maximum between $R_{Ox} = 0.7$ and $R_{Ox} = 3.5$, it rose at $R_{OH} = -0.1$ as the amount of nitrate that was used was increased. In the first case, this was accompanied by a change in morphology. Thus, the particles obtained were pentacontahedral (50 facets) in the lower R_{Ox} -region and dodecahedral (12 facets) in the higher R_{Ox} -region.

In the second case, when nitrite correlates with the amount of nitrate that was used, goethite was also precipitated if the R_{Ox} value was above a certain level. Thus, no goethite was identified until $R_{Ox} = 1.4$. However, from the next test point, which was at $R_{Ox} = 3.5$, the amount of goethite seems to correlate with the amount of nitrate that was employed.

Almost exactly at the transition point $R_{OH} = 0.0$, no indication of goethite was found anymore, even at very high R_{Ox} values. The amount of nitrite determined in the supernatant, however,

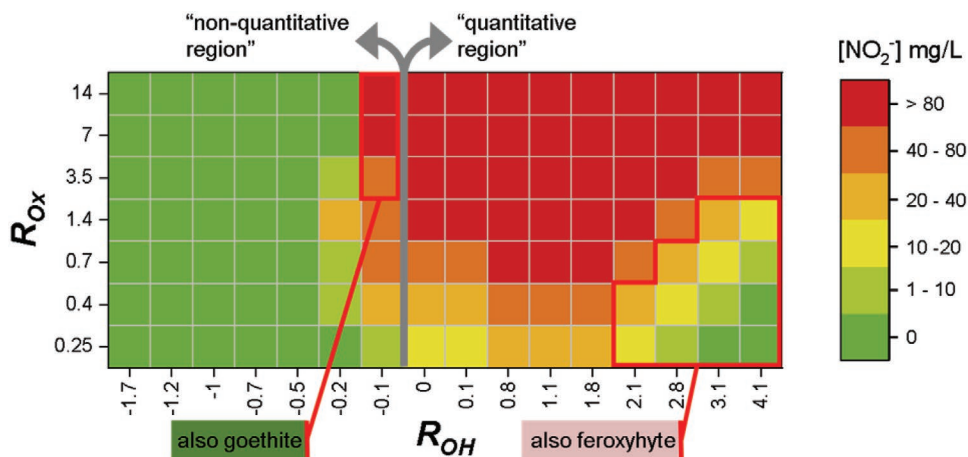


Figure 5. Amount of nitrite, which is determined in the supernatant after completion of the reaction, depending on R_{OH} and R_{Ox} .

still correlates with the amount of nitrate used. This applies in general also to the entire “quantitative region” ($R_{OH} \geq 0.0$). While within this “quantitative region”, in the upper R_{Ox} -region, no further distinctive points become apparent, some observations in the lower R_{Ox} -region could be related to possible transitions: between $0.0 < R_{OH} < 1.0$, the appearance of the obtained particles changes. While they are still octadecahedral at $R_{OH} = 0.0$, they already deform slightly above this point. At first, they are rather dodecahedral-like, later more and more octahedral-like. Since, within this subregion and under otherwise identical conditions, the determined nitrite content increases with increasing R_{OH} , it seems possible that there is a relationship in this respect. In the subsequent subregion, between $1.0 < R_{OH} < 2.0$, almost exclusively relatively large octahedral products dominate. Furthermore, the amount of nitrite determined is almost independent of R_{OH} . This may explain the morphological stability in this subregion. In the next subregion, between $2.0 < R_{OH} < 3.0$, R_{OH} -dependent deformations occur again. Apart from the deformed octahedron-like ones, no other types are clearly recognizable. Lowering R_{Ox} in this sub-region down to $R_{Ox} = 0.25$ now also gives rise to feroxyhyte. Similarly, as before, there seems to be a relation between the amount of nitrite found and the quantity of the precipitated feroxyhyte. The more feroxyhyte was precipitated, the less nitrite was found. In addition, the amount of nitrite generated in the subregion seems also to correlate with the hydroxide that was provided. Thus, under otherwise identical conditions, the determined nitrite concentration decreased with increasing R_{OH} . Consequently, above $R_{OH} = 3.0$, feroxyhyte was the main precipitate within the low R_{Ox} -region, while in the high R_{Ox} -region magnetite was still the exclusive product.

3.5. Magnetic Properties

The saturation magnetization M_S of the magnetic products obtained are all within a range of about 80–90 emu g^{-1} (Figure S6, Supporting Information), which is close to the value of 92–100 emu g^{-1} reported for bulk magnetite.^[40] Variations from this can mostly be associated due to a change in the crystallite size and thus also a change in the magnetic domain size.

For example, the crystallite size in the series $R_{OH} = 0.1$ decreases slightly (starting from a maximum at $R_{Ox} = 0.7$), which implies a reduction in the size of the magnetic domain, thus reducing the saturation magnetization (Figure 6a,b).

However, in the same series, it becomes obvious that there is additionally a strong relationship between the nitrate concentration and the coercivity H_C (Figure 6b). Thus, the coercivity, with a determined value of up to $H_C = 415$ Oe, is quite high within the “stoichiometric region” ($0.4 < R_{Ox} < 1$), but then drops rapidly to a value below $H_C = 100$ as R_{Ox} increases. This cannot be easily related to the crystallite sizes calculated from the XRD, since the values are relatively constant between 40 and 50 nm over the entire R_{Ox} -range (Figure 6a). However, there may be a correlation with the actual particle size that can be observed using SEM (Figure 6a,c). Thus, the particles obtained in the stoichiometric R_{Ox} -region are significantly larger than would be expected from the corresponding XRD values. With increasing R_{Ox} , however, they slowly approach similar values. This fits the assumption that above a certain nitrate concentration, single crystals are obtained. Below this concentration, however, it is more likely that particles will evolve that can be considered as some kind of oriented aggregates with distinct magnetic properties.

Considering the whole parameter range (Figure 6d with respect to the XRD size depicted in Figure S4, Supporting Information), it can be concluded that there are no significant differences below $R_{OH} = 0.0$, although the morphologies differ. Thus, the coercivity in this region is quite low and seems to correlate with the calculated crystallite sizes and the associated expectations. On the other hand, the particles obtained are actually very large (see Figure 2), which at first seems to contradict this. Considering the results so far, two simple explanations may seem reasonable at first glance. On the one hand, the assumption of multi-domains would be quite suitable. However, on the other hand, also aggregated but not strongly interacting, that is, predominantly isolated crystallites could show similar behavior. Both assumptions consider the actual particle size. While the former assumes a more strongly fused matrix and therefore some kind of soft magnetic material, the latter, in contrast, assumes a mesocrystalline-like structure. Taking all data into account, a mesocrystalline structure seems more probable:

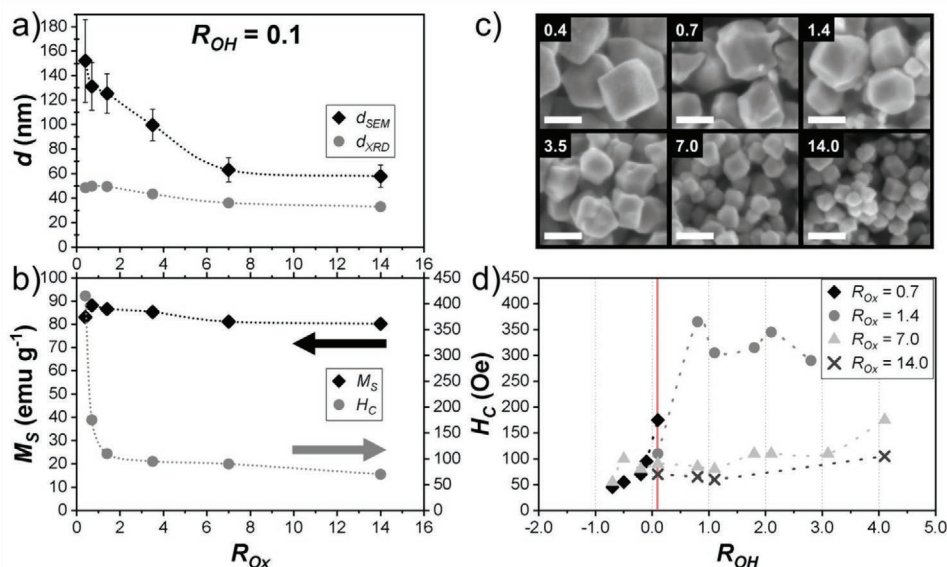


Figure 6. a) Particle sizes determined from corresponding R_{Ox} -related SEM images (c) and the crystallite sizes calculated from the X-ray diffractograms for the “ $R_{OH} = 0.1$ ” series as a function of R_{Ox} . b) Corresponding magnetic properties: coercivity H_C and saturation magnetization M_S . d) Magnetic properties as a function of R_{OH} for several R_{Ox} -series (the red line highlights $R_{OH} = 0.1$, which corresponds to the data shown in detail in (b)).

In comparison, the products obtained above $R_{OH} = 0.0$ show much clearer differences depending on the amount of nitrate used. In general, what has already been discussed for $R_{OH} = 0.1$ can be observed over the entire region. The use of high nitrate concentrations (high R_{Ox}) causes predominantly the generation of single crystals whose size correlates with the size of the magnetic domain and thus also with the coercivity. However, if the amount of nitrate used is low (low R_{Ox}), the magnetic products possess an unexpectedly high coercivity, although the corresponding calculated crystallite sizes do not indicate a correlation. In this region, again, the generated particles are relatively large, although the crystallite size barely changes and retains a comparable size to the other regions. Taking this into account, the product appears to be some kind of hard magnetic material. On the one hand, this could be due to a multi-domain product in which, for example, impurities or defects strongly impede the magnetic domain wall movement. On the other hand, it is also conceivable that the product is an aggregate of smaller crystallites that cannot fuse due to attached molecules but are coupled in such a way that magnetic reorientation requires a simultaneous reorientation of all crystallites. Thus, in a sense, the entire particle appears as a superordinate quasi-single domain, whose magnetic reorientation requires a certain effort, which results in a correspondingly high coercivity. This, again, supports the assumption that these particles are some kind of mesocrystalline products, which fits best to the previous results.

4. Conclusion

Magnetite nanoparticles from iron(II) sulfate were synthesized via oxidative precipitation and the influence of nitrate concentration as a function of hydroxide concentration was investigated. The nitrate concentration plays a decisive role in

particle formation and evolution of their magnetic properties. Based on the findings, it is recommendable to distinguish between a “quantitative region” and a “non-quantitative region”, since the products in these (relatively sharply separated) regions differ considerably in their characteristics. In the “non-quantitative region”, predominantly mesocrystalline structures arise, which can be associated with remaining and probably coordinated sulfate, which presumably prevents further fusion processes. In addition, the mesocrystalline structures differ in their number of facets, depending on how much nitrate was used. In the “quantitative region”, there was no evidence of residual sulfate. Nevertheless, a clear dependence on the nitrate concentration could be determined also in this region: high amounts of nitrate caused the generation of single crystals, whereas low nitrate amounts again caused the generation of mesocrystal-like particles, in which OH groups now seem to act as spacers. All of these morphological differences were also reflected in the magnetic properties: although the saturation magnetizations hardly differed, there were clear differences in coercivity. In the case of the OH-bearing mesocrystals, cooperative effects seem to occur that strongly increase coercivity. Similar indications could not be found in the sulfate-bearing mesocrystals. Although the particles were much larger, their coercivity corresponded in the broadest sense to the crystallite size calculated and could therefore not be magnetically distinguished from those of the single crystals.

5. Experimental Section

Materials: Iron(II) sulfate heptahydrate ($FeSO_4 \cdot 7H_2O$, 99.5%) and potassium nitrate (KNO_3 , 99+%) were obtained from Acros Organics. Potassium hydroxide (KOH, 90%, flakes) was obtained from VWR International. All reagents were used without further purification.

Synthesis: The synthesis was based, slightly modified, on the method of oxidative precipitation described by Sugimoto and Matijevic.^[3]

To minimize effects induced by magnetic fields, for example, chain formation, the synthesis was performed using an overhead stirrer and a heating mantle.^[27,41] Typically, FeSO₄ (20 mM) was dissolved in deionized (135 mL) water and allowed to boil while introducing nitrogen. In parallel, KOH and KNO₃, according to the desired ratios R_{OH} and R_{Ox} , were dissolved together in deionized water (15 mL) at 60 °C, also with the introduction of nitrogen. After about 20 min of conditioning (=time given to reach boiling), the basic oxidation solution was added to the ferrous salt solution. A typical reaction was then allowed to proceed 240 min under reflux, still with nitrogen introduction. After finishing, the reaction mixture was cooled down, sedimented, and washed several times with deionized water for purification.

Qualitative methods: In order to detect ammonia, gases escaping from the reaction were directed over a pH test strip (Dosatest pH test strips, pH 4.5–10.0, VWR International), which changed its color accordingly if a basic gas occurred. In order to estimate how much nitrite was generated due to the nitrate reduction, a semi-quantitative determination was made from the supernatant after the reaction using suitable test strips (QUANTOFIX Nitrate/Nitrite, MACHERY-NAGEL). Non-converted iron, which was still dissolved in the supernatant after the reaction, was quantified colorimetrically using 2,2'-bipyridine as chelator.

Scanning electron microscopy (SEM): To obtain detailed information on particle morphologies, electron micrographs were taken with a Zeiss Supra 25 SEM at 2 kV (field emission) and 2.7 mm working distance, usually using the in-lens detector. Samples were prepared from suspensions on a thin gold plate, which was placed on an SEM sample holder after drying.

FTIR spectroscopy: To obtain information about the composition and surface of the products, infrared spectroscopic measurements of corresponding KBr pellets were performed using a Nicolet MagnaIR 760 from Thermo Fisher Scientific. The spectra were recorded via 64 scans from 4000 to 400 cm⁻¹ at a resolution of 1 cm⁻¹. As background, the spectrum of a pure KBr pellet was used.

Powder XRD: The composition of the obtained products was analyzed by XRD on a PANalytical Empyrean Series 2 with automatic divergence slit using Cu K α radiation. Crystallite size was determined based on the Scherrer equation, taking the average of the sum of the peaks (220) at $2\theta = 30.1^\circ$, (311) at $2\theta = 35.5^\circ$ and (222) at $2\theta = 37.1^\circ$. The wavelength used for calculation was $\lambda = 1.540598 \text{ \AA}$ (Cu K α), the shape factor K was set to 0.94.

Zeta Potential Measurements: To determine the IEPs, zeta potential measurements were performed with a Zetasizer Nano ZS from Malvern Instruments. Therefore the respective particles were dispersed in a 1 mM NaCl solution. HCl respectively NaOH was used to adjust different pH values.

Magnetic Measurements: Magnetic properties of purified and vacuum dried (70 °C, 20 mbar) magnetic particles were studied with a vibrating-sample magnetometer (VSM, VersaLabTM 3T cryogen-free VSM), cycling the applied field from -30 to +30 kOe with a step rate of 50 Oe s⁻¹. Detailed analyses were carried out by cycling the applied field from -3 to +3 kOe with 5 Oe s⁻¹. The temperature was set to 300 K. It should be noted that magnetization values within this work were given in emu g⁻¹ (cgs units) which can be set equal to A m² kg⁻¹ (SI units).

Supporting Information

Supporting Information is available from the Wiley Online Library or from the author.

Acknowledgements

This work was financially supported by the DFG (grant MA 7252/4-2). The authors thank Margit Schubertrügmer for performing SEM analyses. Open access funding enabled and organized by Projekt DEAL.

Conflict of Interest

The authors declare no conflict of interest.

Keywords

colloidal nanostructures, nanoparticle aggregation, non-classical crystallization, oriented attachment

Received: November 25, 2020

Published online: January 15, 2021

- [1] J. Heil, H. Vereecken, N. Brüggemann, *Eur. J. Soil Sci.* **2016**, *67*, 23.
- [2] a) C. J. Ottley, W. Davison, W. M. Edmunds, *Geochim. Cosmochim. Acta* **1997**, *61*, 1819; b) R. J. Buresh, J. T. Moraghan, *J. Environ. Qual.* **1976**, *5*, 320; c) D. Wu, B. Shao, M. Fu, C. Luo, Z. Liu, *Chem. Eng. J.* **2015**, *279*, 149; d) M. T. Inam-Ul-Haque, *J. Chem. Soc. Pak.* **2010**, *32*, 396; e) H. C. B. Hansen, O. K. Borggaard, J. Sørensen, *Geochim. Cosmochim. Acta* **1994**, *58*, 2599.
- [3] T. Sugimoto, E. Matijević, *J. Colloid Interface Sci.* **1980**, *74*, 227.
- [4] M. Wang, R. Hu, J. Zhao, Y. Kuzyakov, S. Liu, *Geoderma* **2016**, *271*, 173.
- [5] M. J. Kampschreur, R. Kleerebezem, W. W. J. M. de Vet, M. C. M. van Loosdrecht, *Water Res.* **2011**, *45*, 5945.
- [6] H. C. B. Hansen, C. Bender Koch, *Clay Miner.* **1998**, *33*, 87.
- [7] a) J. A. Camargo, A. Alonso, A. Salamanca, *Chemosphere* **2005**, *58*, 1255; b) K. Brindha, S. P. Renganayaki, L. Elango, *Indian J. Environ. Prot.* **2017**, *37*, 667; c) E. H. Burden, *Analyst* **1961**, *86*, 429.
- [8] A. E. Ghaly, V. V. Ramakrishnan, *Journal of Pollution Effects & Control* **2015**, *3*, 1.
- [9] X. Zhu-Barker, A. R. Cavazos, N. E. Ostrom, W. R. Horwath, J. B. Glass, *Biogeochemistry* **2015**, *126*, 251.
- [10] J.-P. Jolivet, C. Chanéac, E. Tronc, *Chem. Commun.* **2004**, 481.
- [11] A. A. Olowe, D. Rezel, J. M. R. Génin, *Hyperfine Interact.* **1989**, *46*, 429.
- [12] C. Domingo, R. Rodríguez-Clemente, M. A. Blesa, *J. Colloid Interface Sci.* **1994**, *165*, 244.
- [13] S. J. Oh, S.-J. Kwon, J.-Y. Lee, J.-Y. Yoo, W.-Y. Choo, *Corrosion* **2002**, *58*, 498.
- [14] V. V. Popov, A. I. Gorbunov, *Russ. J. Inorg. Chem.* **2010**, *55*, 1508.
- [15] A. Olowe, B. Pauron, J. Génin, *Corros. Sci.* **1991**, *32*, 985.
- [16] A. Olowe, J.-M. R. Génin, *Corros. Sci.* **1991**, *32*, 965.
- [17] G. Mirabello, A. Ianiro, P. H. H. Bomans, T. Yoda, A. Arakaki, H. Friedrich, G. de With, N. A. J. M. Sommerdijk, *Nat. Mater.* **2020**, *19*, 391.
- [18] T. an Vu, M. M. Reagan, D. Li, B. Legg, J. J. de Yoreo, J. F. Banfield, H. Zhang, *CrystEngComm* **2014**, *16*, 1466.
- [19] a) R. L. Penn, J. A. Soltis, *CrystEngComm* **2014**, *16*, 1409; b) G. Mirabello, A. Keizer, P. H. H. Bomans, A. Kovács, R. E. Dunin-Borkowski, N. A. J. M. Sommerdijk, H. Friedrich, *Chem. Mater.* **2019**, *31*, 7320.
- [20] M. Benz, A. Brune, B. Schink, *Arch. Microbiol.* **1998**, *169*, 159.
- [21] U. Schwertmann, L. Carlson, H. Fechter, *Aquat. Sci.* **1984**, *46*, 185.
- [22] a) T. L. Theis, P. C. Singer, *Environ. Sci. Technol.* **1974**, *8*, 569; b) A. M. Jones, P. J. Griffin, T. D. Waite, *Geochim. Cosmochim. Acta* **2015**, *160*, 117; c) J. Jing, Y. Zhang, J. Liang, Q. Zhang, E. Bryant, C. Avendano, V. L. Colvin, Y. Wang, W. Li, W. W. Yu, *J. Nanopart. Res.* **2012**, *14*, 827; d) T. J. Strathmann, in *ACS Symposium Series*, Vol. 1071 (Eds: P. G. Tratnyek, T. J. Grundl, S. B. Haderlein), American Chemical Society, Washington, DC, **2011**, pp. 283–313.
- [23] H. Guo, A. S. Barnard, *J. Mater. Chem. A* **2013**, *1*, 27.
- [24] a) J. Kielemoes, P. de Boever, W. Verstraete, *Environ. Sci. Technol.* **2000**, *34*, 663; b) Y. H. Huang, T. C. Zhang, *Chemosphere* **2006**, *64*, 937; c) M. Stratmann, *Ber. Bunsen-Ges.* **1990**, *94*, 626.

- [25] a) D. Koziej, A. Lauria, M. Niederberger, *Adv. Mater.* **2014**, *26*, 235; b) M. Usman, J. M. Byrne, A. Chaudhary, S. Orsetti, K. Hanna, C. Ruby, A. Kappler, S. B. Haderlein, *Chem. Rev.* **2018**, *118*, 3251; c) A. A. Jelle, M. Hmadeh, P. G. O'Brien, D. D. Perovic, G. A. Ozin, *ChemNanoMat* **2016**, *2*, 1047.
- [26] a) O. Baudisch, L. A. Welo, *J. Biol. Chem.* **1925**, *64*, 753; b) O. Baudisch, *J. Biol. Chem.* **1921**, *48*, 489.
- [27] F. Vereda, J. d. Vicente, R. Hidalgo-Álvarez, *Langmuir* **2007**, *23*, 3581.
- [28] Y. Zhang, Z. Ren, Y. Fu, X. Yuan, Y. Zhai, H. Huang, H. Zhai, *J. Phys. Chem. Solids* **2009**, *70*, 505.
- [29] F. Vereda, M. P. Del Morales, B. Rodríguez-González, J. de Vicente, R. Hidalgo-Alvarez, *CrystEngComm* **2013**, *15*, 5236.
- [30] a) Y. Luengo, M. d. P. Morales, L. Gutiérrez, S. Veintemillas-Verdaguer, *J. Mater. Chem. C* **2016**, *4*, 9482; b) N. Amin, S. Arajs, E. Matijević, *Phys. Status Solidi A* **1987**, *101*, 233; c) P. S. Sidhu, R. J. Gilkes, A. M. Posner, *J. Inorg. Nucl. Chem.* **1978**, *40*, 429; d) A. Simon, H.-H. Emons, *J. Prakt. Chem.* **1961**, *13*, 163.
- [31] M. A. Vergés, R. Costo, A. G. Roca, J. F. Marco, G. F. Goya, C. J. Serna, M. d. P. Morales, *J. Phys. D: Appl. Phys.* **2008**, *41*, 134003.
- [32] F. Vereda, J. d. Vicente, R. Hidalgo-Álvarez, *J. Colloid Interface Sci.* **2013**, *392*, 50.
- [33] A. Simon, H.-H. Emons, *J. Prakt. Chem.* **1961**, *13*, 106.
- [34] B. Weckler, H. D. Lutz, *Eur. J. Solid State Inorg. Chem.* **1998**, *35*, 531.
- [35] Y.-S. Li, J. S. Church, A. L. Woodhead, *J. Magn. Magn. Mater.* **2012**, *324*, 1543.
- [36] H. C. Liese, *Am. Mineral.* **1967**, *52*, 1198.
- [37] a) J.-F. Boily, P. L. Gassman, T. Peretyazhko, J. Szanyi, J. M. Zachara, *Environ. Sci. Technol.* **2010**, *44*, 1185; b) M. D. Lane, *Am. Mineral.* **2007**, *92*, 1.
- [38] a) J. Madejová, J. Kečkéš, H. Pálková, P. Komadel, *Clay Miner.* **2002**, *37*, 377; b) J. Bishop, J. Madejová, P. Komadel, H. Fröschl, *Clay Miner.* **2002**, *37*, 607.
- [39] M. Kosmulski, *Adv. Colloid Interface Sci.* **2016**, *238*, 1.
- [40] *The Iron Oxides: Structure, Properties, Reactions, Occurrences and Uses* (Eds: R. M. Cornell, U. Schwertmann), Wiley-VCH, Weinheim, Germany **2003**.
- [41] J. J. Brunner, M. Krumova, H. Cölfen, E. V. Sturm Née Rosseeva, *Beilstein J. Nanotechnol.* **2019**, *10*, 894.